JACS
JOURNAL OF THE AMERICAN CHEMICAL SOCIETY
Article
pubs.acs.org/JACS

Fabrication of a Core–Shell-Type Photocatalyst via Photodeposition of Group IV and V Transition Metal Oxyhydroxides: An Effective Surface Modification Method for Overall Water Splitting

Tsuyoshi Takata,*[,†] Chengsi Pan,[†] Mamiko Nakabayashi,[‡,∥] Naoya Shibata,[‡] and Kazunari Domen*[,†,§,∥]

[†]Global Research Center for Environment and Energy based on Nanomaterials Science (GREEN), National Institute for Materials Science (NIMS), 1-1 Namiki, Tsukuba-city, Ibaraki 305-0044, Japan

[‡]Institute of Engineering Innovation, School of Engineering, The University of Tokyo, 2-11-16, Yayoi, Bunkyo-ku, 113-8656, Japan

[§]Department of Chemical System Engineering, School of Engineering, The University of Tokyo, 7-3-1 Hongo, Bunkyo-ku 113-8656, Japan

[∥]Japan Technological Research Association of Artificial Photosynthetic Chemical Process (ARPChem), 5-1-5 Kashiwanoha, Kashiwa-city, Ciba 227-8589, Japan

Supporting Information

ABSTRACT: The design of optimal surface structures for photocatalysts is a key to efficient overall water splitting into H_2 and O_2. A unique surface modification method was devised for a photocatalyst to effectively promote overall water splitting. Photodeposition of amorphous oxyhydroxides of group IV and V transition metals (Ti, Nb, Ta) over a semiconductor photocatalyst from corresponding water-soluble metal peroxide complexes was examined. In this method, amorphous oxyhydroxide covered the whole surface of the photocatalyst particles, creating a core–shell structure. The water splitting behavior of the novel core–shell-type photocatalyst in relation to the permeation behavior of the coating layer was investigated in detail. Overall water splitting proceeded successfully after the photodeposition, owing to the prevention of the reverse reaction. The photodeposited oxyhydroxide layers were found to function as molecular sieves, selectively filtering reactant and product molecules. By exploiting the selective permeability of the coating layer, redox reactions on the photocatalyst surface could be suitably controlled, which resulted in successful overall water splitting.

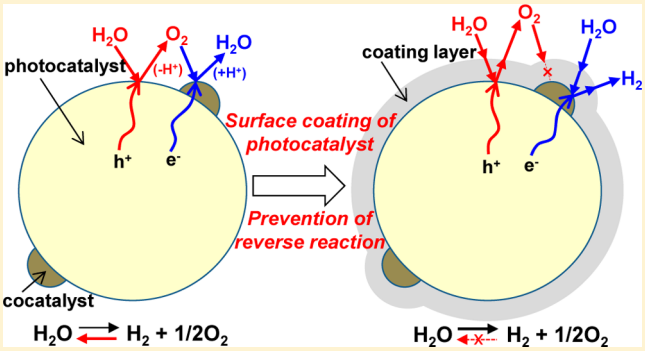

INTRODUCTION

Photocatalytic overall water splitting into hydrogen and oxygen is expected to become a widely used method for obtaining clean and renewable energy. In order to harness solar energy efficiently, various photocatalysts with relatively narrow bandgaps have been intensively developed. The main approach has been to design the electronic band structure of semiconductor materials with suitable optical absorption, reduction and oxidation abilities, and photocarrier mobility, primarily by compositional tuning, and thus numerous studies on the development of new semiconductor materials as photocatalysts have been reported.[1−3]

Cocatalysts also play a critical role in enabling overall water splitting by controlling the redox reactions on the surface of photocatalysts. Despite numerous reports on new semiconductor photocatalyst materials, relatively few effective cocatalysts for overall water splitting have been reported. We believe that this cocatalyst shortage has been the main factor hindering progress in this area. Recently, various new catalysts capable of promoting electrochemical hydrogen evolution[4−8] or water oxidation[8−11] have been reported. However, in practice, these electrocatalysts are not directly applicable to overall water splitting using a particulate photocatalyst. This is likely because such catalysts are usable in an irreversible electrolysis system but are not effective in the form of a particulate photocatalyst based on a reversible process, primarily owing to the concurrent reverse reaction. It is clear that merely the combination of a suitable semiconductor and electrochemically active material does not necessarily lead to successful photocatalytic overall water splitting. Thus, strategic approaches targeting the fabrication of cocatalysts for overall water splitting that will be functional on particulate photocatalysts are needed.

Successful examples of cocatalysts include cases where overall water splitting has been achieved by dispersing metal or metal oxide nanoparticles on the surface of photocatalyst particles. It is thought that cocatalyst components like Pt,[12] Ni,[13] Rh,[14] and Ru[15] can promote H_2 evolution because of their lower

Received: April 21, 2015
Published: July 10, 2015

DOI: 10.1021/jacs.5b04107
J. Am. Chem. Soc. 2015, 137, 9627−9634

overpotentials, while they are also active for the oxygen reduction reaction (ORR), which corresponds to the reverse of the water splitting reaction. Thermodynamically, the latter reaction is dominant, and thus, water splitting tends to be obstructed. Overall water splitting has been achieved by preventing the concurrent ORR, but such examples of cocatalysts remain limited in number.[12−18]

We have previously demonstrated a methodology and identified the mechanism for effectively preventing the ORR on a H_2 evolution cocatalyst: the addition of Cr^{3+} species as a second cocatalyst component.[19−21] Coating the whole surface of each cocatalyst nanoparticle with a hydrated Cr_2O_3 thin layer to form a core−shell-type cocatalyst proves effective for overall water splitting. The hydrated Cr_2O_3 layer hinders the access of evolved O_2 molecules to the surface of the H_2 evolution sites, i.e., the external surface of the core, from the outside. On the other hand, the reactant H_2O molecules or H^+ ions can reach the surface of the cocatalyst by permeation, but the H_2 molecules produced can be released outside the layer, as illustrated in Figure 1.[22] Such selective permeability enables the prevention of the ORR as well as the occurrence of overall water splitting.

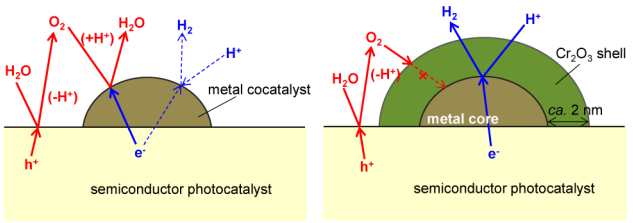

Figure 1. Schematic of the function of the core−shell-structured cocatalyst.

Although the addition of Cr species as a second cocatalyst component has been effective for various semiconductor photocatalysts with relatively wide bandgaps (>ca. 2.5 eV),[20,23,24] overall water splitting has not been achieved in the case of narrower-bandgap (<ca. 2.5 eV) materials. To achieve overall water splitting on photocatalysts with narrower bandgaps, we explored novel surface modification methods that could offer an alternative to the Cr system.

In the formation of a core−shell-structured cocatalyst, $Cr(III)_2O_3$ can be deposited on the surface of the H_2 evolution cocatalyst by reducing $Cr(VI)O_4^{2-}$ ions with photoexcited electrons, through a mechanism similar to electroplating, as expressed by eqs 1−3.

Reduction step:

$$K_2Cr(IV)O_4 + 3e^- + 3H^+ \rightarrow 1/2Cr(III)_2O_3 + 1/2H_2O + 2KOH \quad (1)$$

Oxidation step:

$$3/2H_2O + 3h^+ \rightarrow 3/2O_2 + 3H^+ \quad (2)$$

Overall reaction:

$$K_2Cr(VI)O_4 + H_2O + 3(e^- + h^+) \rightarrow 1/2Cr(III)_2O_3 + 3/2O_2 + 2KOH \quad (3)$$

By analogy with this mechanism, alkaline oxometalates involving transition metals with uncommonly high valence states like $LiNi(III)O_2$, $LiCo(III)O_2$, $Na_2Fe(IV)O_3$,[25] $Na_2Fe(VI)O_4$,[25] and $KMn(VII)O_4$ are considered to be precursor candidates for depositing metal oxides with common valence states like $Ni(II)O$, $Co(II,III)_3O_4$, $Fe(III)_2O_3$, and $Mn(II,III)O_x$. However, no suitable precursors for photodeposition that can replace chromate have been found among these oxometalates for various reasons, e.g., difficulty in synthesis, instability, and water-insolubility.

Recently, we devised a novel method for the photodeposition of Ti oxyhydroxide from a water-soluble Ti peroxide complex. Generally, oxides of Ti^{4+}, Nb^{5+}, and Ta^{5+} are not soluble in aqueous solutions over a wide pH range. However, it is widely known that these oxides can dissolve in an aqueous H_2O_2 solution by forming water-soluble metal peroxide complexes. The peroxo ligands of these complexes are in the O^- state. Therefore, electron injection from a photoexcited semiconductor to the O^- state should be easy. Photoexcitation of a semiconductor photocatalyst in an aqueous metal peroxide solution is expected to result in the facile decomposition of a metal peroxide complex as well as the deposition of a metal (M = Ti, Nb, Ta) oxyhydroxide layer on the surface of the cocatalyst, along with the liberation of O_2 via eq 4.

$$M(OH)_x O_y (O_2)_z \cdot nH_2O + z(e^- + h^+) \rightarrow M(OH)_{x'} O_{y'} \cdot n'H_2O + zO_2 \quad (4)$$

By using this photodeposition method, we were able to achieve overall water splitting on a transition metal oxynitride, $LaMg_{1/3}Ta_{2/3}O_2N$, with a bandgap of 2.08 eV. Our brief results on this new photocatalyst and photodeposition method have been reported recently.[26] We initially intended to develop a core-sell-type cocatalyst in which the Cr_2O_3 shell would be replaced by an alternative material. However, it was found that the photodeposited material covered the whole surface of the photocatalyst particles, creating not a core−shell-type cocatalyst, but a core−shell-type photocatalyst. In the present paper, we investigated the photocatalytic behaviors of a surface coated photocatalyst in detail to reveal the functions of the surface modification. To gain broad insight into the design of water splitting photocatalysts, one of the most well-known photocatalysts, $SrTiO_3$ (E_g = 3.2 eV), was chosen as a model sample.

EXPERIMENTAL SECTION

In the present experiments, $SrTiO_3$ doped with a lower valence cation was employed, because a markedly higher photocatalytic activity compared to that of undoped $SrTiO_3$ could be obtained with good reproducibility.[27] $SrTiO_3$ in which 5 at% of the Ti^{4+} at the B-site of the perovskite was substituted with Sc^{3+} (hereafter "$SrTiO_3$:Sc", details in Supporting Information SI1) was prepared from a thoroughly ground stoichiometric mixture of TiO_2, $SrCO_3$, and Sc_2O_3 (Kanto Chemical Co.; all chemicals used were analytical grade) by a 20 h solid state reaction at 1373 K in air.

The as-synthesized photocatalyst was variously modified by depositing a cocatalyst and a coating layer. In this manuscript, the amount of deposition is expressed by the weight of the deposit per weight of photocatalyst. Rh_2O_3 (0.5 wt %) was loaded on $SrTiO_3$:Sc from $RhCl_3$ (Kanto Chemical Co.) by an impregnation method. The $SrTiO_3$:Sc powder was immersed in a small amount of H_2O containing $RhCl_3$ and then dried on a hot water bath, followed by heating in air at 623 K for 1 h.

Then, the photocatalyst was further modified by photodepositing a metal oxyhydroxide as a coating layer. The photodeposited materials likely contained water and occurred as oxyhydroxides, but for simplicity, they will be referred to as oxides hereafter. Aqueous solutions of metal peroxide complexes as precursors for photodeposition were prepared according to the following procedure.

DOI: 10.1021/jacs.5b04107
J. Am. Chem. Soc. 2015, 137, 9627−9634

Amorphous TiO_2 was first prepared by just hydrolysis of titanium tetraisopropoxide (Kanto Chemical Co.), employed as a Ti source. Typically, for the photodeposition of TiO_2 (3 wt % as TiO_2), 3 mg of as-prepared TiO_2 was added to 0.5 mL of H_2O_2 aqueous solution (Kanto Chemical Co., 30−35 wt %), followed by sonication for a few minutes. Sonication was repeated several times with several-minute intervals in between to obtain a pale yellow solution. The solution at this stage will be referred to as Ti-peroxide solution (A). Then, a 1 M NaOH solution was added so that the Na:Ti molar ratio became 2:1, yielding a colorless transparent solution, which will be referred to as Ti-peroxide solution (B). The former solution was used to deposit TiO_2 by the impregnation method, while the latter was used for photodeposition. Ta- and Nb-peroxide solutions were prepared according to a procedure similar to that used to prepare the Ti-peroxide solution. Typically, for the photodeposition of Ta_2O_5 or Nb_2O_5 (5 and 4 wt %, respectively), 8.1 mg of $TaCl_5$ or 4.9 mg of $NbCl_5$ (3N Kojundo Chemical Laboratory Co.) was added to 0.5 mL of aqueous H_2O_2 solution, followed by the addition of 1 M NaOH solution (Ta,Nb:Na = 1:5) and brief sonication, yielding a colorless transparent solution.[28] The molar amount of H_2O_2 contained in the aqueous peroxide solution was approximately 2 orders of magnitude larger than those of the metal peroxides. Note that these peroxide solutions are stabilized only in the presence of excess H_2O_2. As-prepared peroxide solutions were directly added into the photocatalytic reaction solution, followed by photoirradiation with a Xe lamp (300 W, full arc).

The photocatalytic reaction was carried out with a reaction vessel made of Pyrex connected to a closed gas circulation system. The reaction vessel was soaked in an outer vessel in which cooling water circulated to keep the temperature of the reaction solution at room temperature. 0.1 g of the as-prepared photocatalyst was dispersed in 250 mL of H_2O containing a certain amount of the metal peroxide solution. The reaction system was evacuated to remove the air in the system and subsequently irradiated by a Xe lamp (300 W, full arc). Evolved gases were analyzed by gas chromatography (Thermal conductivity detector, Ar carrier, Molecular sieve-5A column).

The structures of the photodeposited samples were analyzed by X-ray diffraction (XRD, Cu Kα radiation, D8 ADVANCE, BRUKER AXS Co., Ltd.), field-emission scanning electron microscopy (FE-SEM, SU-8020, Hitachi High-Technologies Corp.), field-emission (scanning) transmission electron microscopy (FE-TEM/STEM, JEM-2800F, JEOL Ltd.) equipped with energy dispersive X-ray spectroscopy (EDS, EX-24055JGT, JEOL Ltd.), X-ray photoelectron spectroscopy (XPS, AXIS-NOVA, Shimadzu Corp.) and inductively coupled plasma-atomic emission spectrometry (ICP-AES, IRIS Advantage, Thermo Fisher Scientific Co., Ltd.).

RESULTS AND DISCUSSION

1. Water Splitting on Various Surface-Modified Samples. *1.1. Effect of Photodeposition on Water Splitting Behavior.* Figure 2 shows the results of photocatalytic reactions with various modifications. Although simultaneous H_2 and O_2 evolution on Rh_2O_3-loaded $SrTiO_3$:Sc was confirmed, its activity was very low (see Figure 2a), likely due to the rapid backward reaction. When $Rh_2O_3/SrTiO_3$:Sc was photoirradiated in the presence of Ti-, Nb-, or Ta-peroxide complexes, a considerable amount of O_2 evolved during the initial 1 or 2 h in each case, as shown in Figure 2b−d. Most of this was due to the decomposition of the added peroxide species, i.e., H_2O_2 and the metal peroxide complex. Among them, the decomposition of H_2O_2 was mostly responsible for the O_2 production because of the much larger H_2O_2 content than the metal peroxide. Then, the rate of O_2 evolution decreased significantly even though O_2 evolution continued. By contrast, in the case of H_2 evolution, an induction period of 1−2 h was observed in each case, after which H_2 evolution continued steadily at a much higher rate than that without photodeposition. These results suggest that

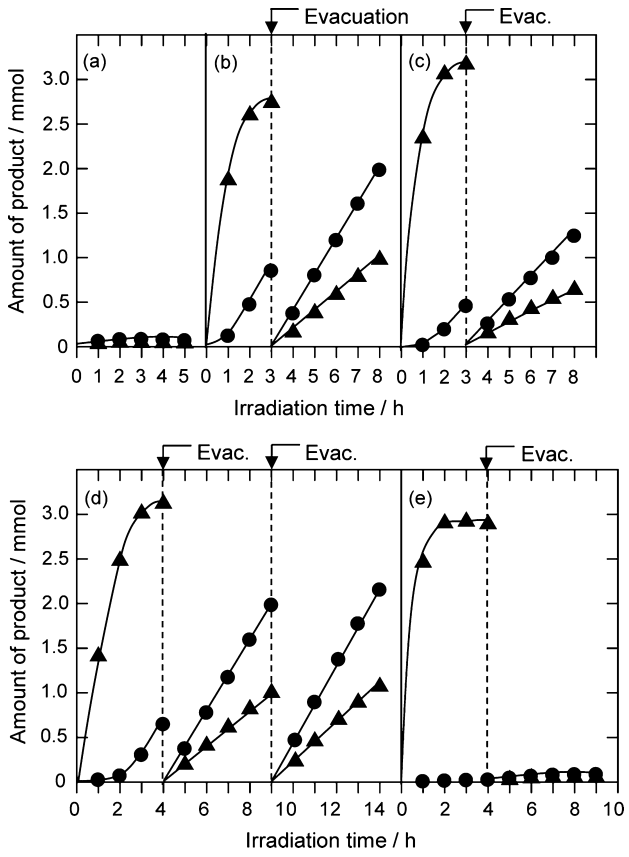

Figure 2. Time courses of gas evolution during photoirradiation of the Rh_2O_3 (0.5 wt %)/$SrTiO_3$:Sc photocatalyst under various conditions: (a) reacted in pure water, (b) TiO_2(3 wt %) photodeposition, (c) Nb_2O_5 (4 wt %) photodeposition, (d) Ta_2O_5 (5 wt %) photodeposition, and (e) reacted in aqueous H_2O_2 solution. Catalyst, 0.1 g; solution, H_2O (250 mL); light source, Xe lamp (300 W, full arc). Filled circles, H_2; filled triangles, O_2.

the decomposition of peroxide species initially occurred preferentially over water splitting because of the instability of the peroxides; water splitting started after the peroxide species in the solution were nearly exhausted. Since the photodeposition process was completed after 3−4 h, photoirradiation was restarted after evacuating the accumulated gases in the reaction system. Then, H_2 and O_2 were produced at constant rates and at the stoichiometric ratio of water splitting, demonstrating that overall water splitting was underway. The rates of H_2 evolution before and after the evacuations were almost the same in each case, which indicates that the evolved O_2 accumulated in the reaction system did not affect H_2 evolution. This reaction behavior proves that ORR was successfully prevented on the Rh_2O_3 cocatalyst by the photodeposition of Ti-, Nb-, or Ta-oxide.

The photocatalytic reaction was also conducted by adding only H_2O_2, without any metal source for photodeposition. Here, the same amount of H_2O_2 was added as in the case of the former experiments shown in Figure 2b−d. As seen in Figure 2e, during the first run, only O_2 evolution occurred, due to the decomposition of H_2O_2, and stopped after 3−4 h of irradiation. The amount of evolved O_2 in this experiment (2.85 mmol) almost matched the amount of H_2O_2 added (ca. 5.0−5.8 mmol). Only small amounts of H_2 and O_2 were generated in the second run, which was almost the same as in the case shown in Figure 2a, where $Rh_2O_3/SrTiO_3$:Sc was irradiated in

DOI: 10.1021/jacs.5b04107
J. Am. Chem. Soc. 2015, 137, 9627−9634

pure water. This result rules out the possibility that the observed overall water splitting was due to any changes caused by the interaction between H_2O_2 and the photocatalyst, and indicates that the photodeposition of metal oxides was essential for overall water splitting.

Prolonged irradiation runs were conducted to examine the stability of the surface coated photocatalyst, $Ta_2O_5/Rh_2O_3/SrTiO_3$:Sc. During 50 h of irradiation, H_2 and O_2 evolution continued steadily without noticeable deactivation, which indicates the stability of the coating structure (see Supporting Information Figure S2).

1.2. Comparison of Rh−Cr and Rh−Ti Binary Cocatalysts. Table 1 compares the effect of additions of Ti- and Cr-species

Table 1. Photocatalytic Activity of $SrTiO_3$:Sc with the Bimetallic Cocatalysts Rh−Cr and Rh−Ti[a]

	activity/μmol h^{-1}	
cocatalyst	H_2	O_2
Rh_2O_3	2	1.9
Cr_2O_3/Rh_2O_3	324	165
$RhCrO_x$	344	176
TiO_2/Rh_2O_3	403	203
$RhTiO_x$	121	65

[a]Catalyst, 0.1 g; solution, H_2O (250 mL); light source, Xe lamp (300 W, full arc). Loading amounts: Rh_2O_3, 0.5 wt %; Cr_2O_3/Rh_2O_3, 1 wt %/0.5 wt %; $RhCrO_x$, 0.5 wt % + 0.5 wt %; TiO_2/Rh_2O_3, 3 wt %/0.5 wt %; $RhTiO_x$, 0.5 wt %+1 wt %.

as a second cocatalyst component on the promotion of overall water splitting. For the Rh−Cr binary cocatalyst system, two types of active phases are known. One is the core−shell-type with a Rh core and Cr_2O_3 shell,[21] which can be fabricated via two-step photodeposition. We note that Rh oxide is also active for the core material (hereafter "Cr_2O_3/Rh_2O_3").[29] The other active phase is a complex oxide of Rh_2O_3 and Cr_2O_3 (hereafter "$RhCrO_x$") fabricated via coimpregnation.[30] It is known that both of these phases have similar effects on the promotion of overall water splitting, despite their different structures. TiO_2-photodeposited $Rh_2O_3/SrTiO_3$:Sc (i.e., the TiO_2/RhO_3-loading) showed somewhat higher photocatalytic activity than the two Rh−Cr binary cocatalyst systems. For coloading of TiO_2 and Rh_2O_3 (i.e., the $RhTiO_x$-cocatalyst) by coimpregnation, Ti-peroxide solution (A) was used. The loading of $RhTiO_x$-cocatalyst lowered the photocatalytic activity substantially compared to other binary cocatalyst systems, but it was noticeably superior to Rh_2O_3-loading alone. Note that the modification conditions were not completely optimized in any of these cases; therefore, the order of the activities could change. However, it can be suggested from these results that the present photodeposition method can promote overall water splitting to an extent similar or superior to the Cr_2O_3 cocatalyst systems. The use of Rh as a cocatalyst core was also examined. In this case, overall water splitting proceeded efficiently after the photodeposition of a coating layer, similarly to the case of Rh_2O_3 core (details in Supporting Information SI3). Our results demonstrate that group IV and V transition metal oxides can be alternatives to Cr_2O_3, which could dispense with the use of Cr^{6+} or Cr^{3+} species, a toxic material or a source of toxic material, respectively.

1.3. Effect of Cocatalyst on Photodeposition Behavior. Next, the photodeposition of Ta_2O_5 was examined on Rh_2O_3-loaded, $RhCrO_x$-loaded, and bare photocatalysts. Figure 3

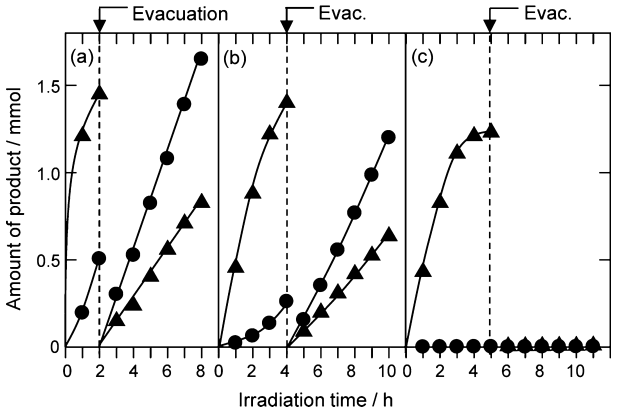

Figure 3. Time courses of gas evolution during photodeposition of Ta_2O_5 (2 wt %) and the subsequent water splitting reactions on variously modified $SrTiO_3$:Sc. (a) Rh_2O_3 (0.5 wt %)-loaded, (b) $RhCrO_x$ (0.5 + 0.5 wt %)-loaded and (c) nonloaded. Catalyst, 0.1 g; solution, H_2O (250 mL); light source, Xe lamp (300 W, full arc). Filled circles, H_2; filled triangles, O_2.

shows the time courses of gas evolution during the photodeposition process and subsequent water splitting reaction on these three samples. When the water splitting process was compared, Rh_2O_3- and $RhCrO_x$-loaded samples (Figure 3a and 3b, respectively) could achieve overall water splitting after Ta_2O_5 deposition, while Ta_2O_5 deposition on the unmodified sample (Figure 3c) clearly failed in water splitting. The Rh_2O_3-loaded sample showed a somewhat superior photocatalytic activity for water splitting compared to the $RhCrO_x$-loaded sample.

The O_2 evolution rate on the Rh_2O_3-loaded sample during the photodeposition process was higher than those of the $RhCrO_x$-loaded and bare samples, whose O_2 evolution rates were comparable. These results indicate that the $RhCrO_x$ cocatalyst and the bare $SrTiO_3$:Sc surface are less active for the decomposition of peroxide species than the Rh_2O_3 cocatalyst. Our previous study revealed that Cr_2O_3 addition selectively prevented reactions other than H_2 evolution.[19] Therefore, it is thought that Cr species substantially suppressed the activity of Rh species for the decomposition of peroxide species. In addition, the decomposition of peroxides also took place on the bare $SrTiO_3$:Sc surface, although the decomposition rate is far lower than that on the Rh_2O_3 cocatalyst surface. This also suggests that Ta_2O_5 was deposited on both Rh_2O_3 and the bare surface of $SrTiO_3$:Sc.

It should be noted that the decomposition of peroxides could occur via the direct photoexcitation of peroxides. The feasibility of this route was experimentally examined and discussed (see Supporting Information SI4). It was confirmed that the direct photoexcitation route was involved in the decomposition of peroxides to only a small extent, and the route via photocatalyst excitation predominated in the photodeposition process.

2. Characterization of Surface Structure. The surface structures of the photodeposited samples were investigated by SEM and XPS. As seen from the high-resolution SEM images in Figure 4a, well-crystallized $SrTiO_3$:Sc particles with smooth surfaces and highly dispersed Rh_2O_3 nanoparticles were observed. On the surface of the 2-wt %-Ta_2O_5-deposited sample, sparsely distributed nanosized deposits were observed that resulted in a rough surface morphology (see Figure 4b). At 5 wt % deposition (Figure 4c), the deposits were densely dispersed and the surface morphology seemed considerably

DOI: 10.1021/jacs.5b04107
J. Am. Chem. Soc. 2015, 137, 9627−9634

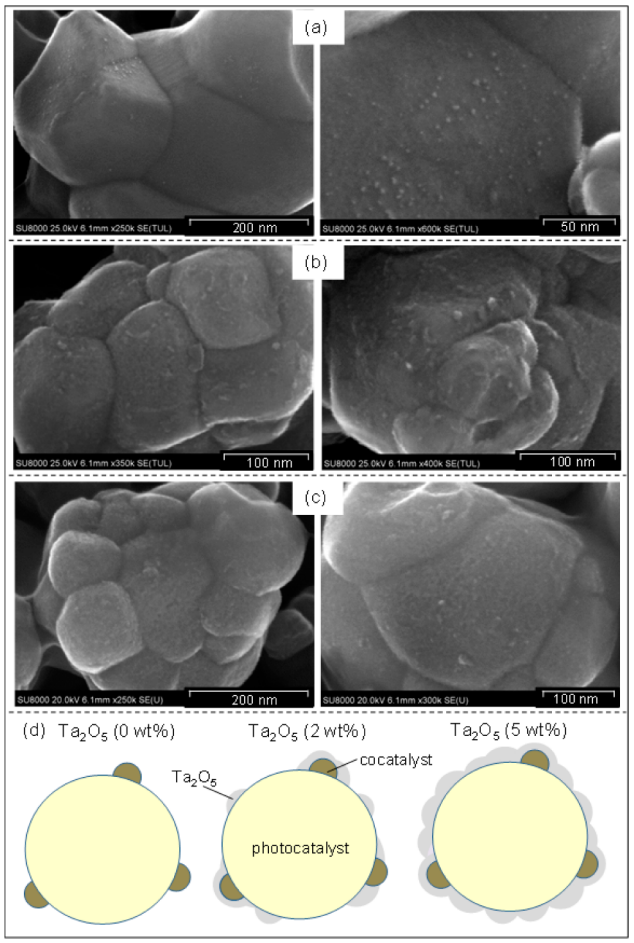

Figure 4. SEM micrographs of (a) Rh_2O_3 (0.5 wt %)/$SrTiO_3$:Sc, (b) Ta_2O_5 (2 wt %)/Rh_2O_3 (0.5 wt %)/$SrTiO_3$:Sc, and (c) Ta_2O_5 (5 wt %)/Rh_2O_3 (0.5 wt %)/$SrTiO_3$:Sc. (d) Schematic of morphological changes.

smoother compared to the 2-wt %-deposited sample, suggesting a fully coated surface, i.e., a core−shell-structured photocatalyst. Figure 4d schematizes the observed morphological changes, which depend on the deposition amount.

The structure of the coating layer was investigated in further detail by HRTEM and STEM-EDS elemental mapping. As seen from Figure 5a, HRTEM images of Ta_2O_5 photodeposited Rh_2O_3/$SrTiO_3$:Sc revealed that an amorphous layer with a few nanometers thickness covered the surface of crystalline $SrTiO_3$:Sc particles. STEM-EDS elemental mapping confirmed that Ta species was broadly dispersed on the whole surface of $SrTiO_3$:Sc particles, creating a core−shell-structured photocatalyst (see Figure 5b).

An XPS analysis was conducted to measure the surface compositions of samples before and after photodeposition of Ta_2O_5 (5 wt %) (details in Supporting Information Figure S5 and Table S1). A Ta peak was clearly detected after photodeposition, whereas those of other metal components decreased. This also supports the formation of a surface-coated structure.

XRD showed that the samples had a diffraction pattern assignable to the single-phase perovskite structure in their pristine form as well as after considerable (15 wt %) Ta_2O_5 photodeposition (see Supporting Information Figure S6). This also indicates that the deposited material was amorphous and

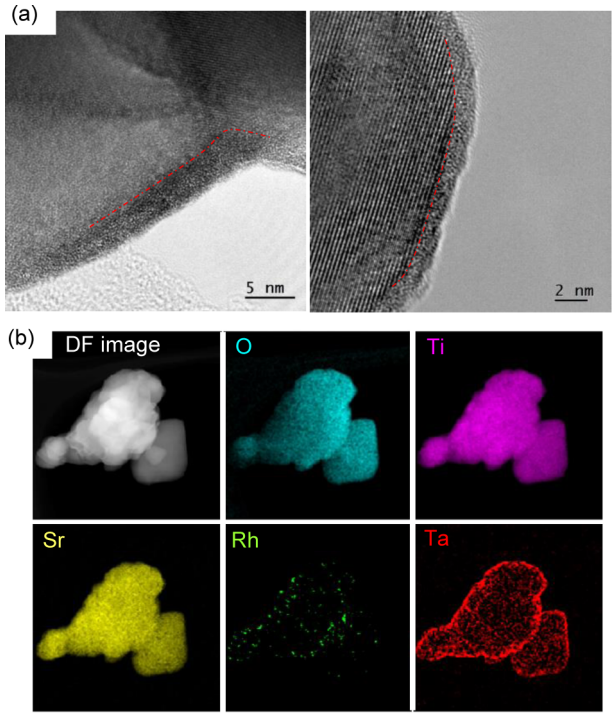

Figure 5. HRTEM micrographs (a) and STEM-EDS elemental mapping (b) of Ta_2O_5 (5 wt %)/Rh_2O_3 (0.5 wt %)/$SrTiO_3$:Sc.

no obvious changes occurred in the structure of $SrTiO_3$:Sc during photodeposition process.

In the case of Cr_2O_3 photodeposition, CrO_4^{2-} ions can be reduced only on the surface of the cocatalyst, which enables selective Cr_2O_3 deposition onto the cocatalyst surface to create a core−shell-structured cocatalyst.[21] However, the peroxide complexes could be decomposed not only on the cocatalyst surface but also on the bare surface of photocatalyst particles. This can explain the observed formation of the core−shell-structured photocatalyst. This mechanism will be discussed in further detail below.

3. Relationship between Permeation Behavior and Photocatalysis. *3.1. Photocatalytic Reaction in Aqueous EtOH Solution.* The photocatalytic reaction behavior was examined in further detail in relation to the permeation behavior of the coating layer. We will address the question of how O_2 evolution via water oxidation is possible on such a fully surface-coated structure. The tentative explanation we gave in our previous report was that water splitting occurred via the reaction with permeating water molecules. However, there was no evidence for this explanation at that stage. A characteristic of the photocatalytic reaction behavior of the fully surface-coated photocatalyst sheds light on this question: the unusual photocatalysis in the presence of EtOH. As shown in Figure 6a-i, Rh_2O_3/$SrTiO_3$:Sc evolved only H_2, which is quite normal. In contrast, notably, Ta_2O_5(5 wt %)-photodeposited Rh_2O_3/$SrTiO_3$:Sc evolved both H_2 and O_2, although the amount of O_2 was slightly smaller than the stoichiometric value, as shown in Figure 6a-ii. In the case of the photocatalytic reaction in aqueous EtOH as a hole scavenger, photoexcited electrons reduce H^+ to form H_2, whereas holes preferentially oxidize EtOH rather than H_2O, and thus no O_2 evolution occurs in almost all cases. However, a nearly stoichiometric amount of O_2 evolved on the surface-coated sample. The only reasonable interpretation for this observation is as follows. The deposited

DOI: 10.1021/jacs.5b04107
J. Am. Chem. Soc. 2015, 137, 9627−9634

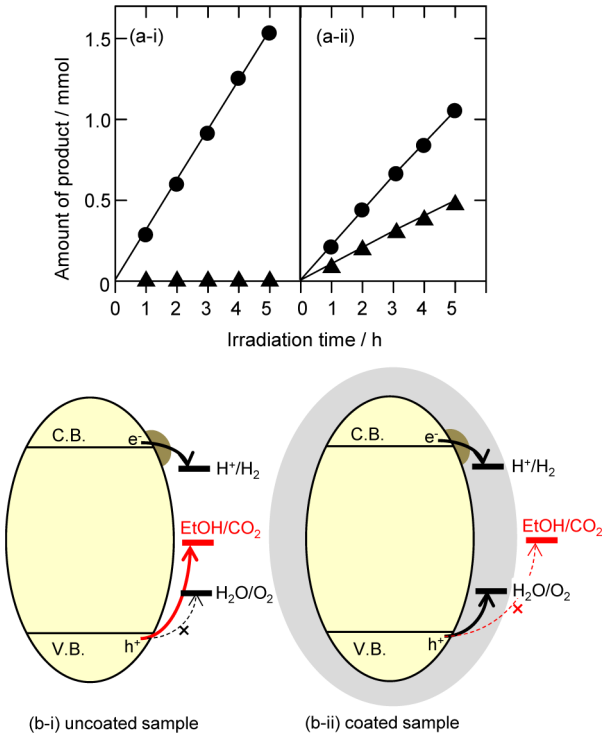

Figure 6. Time courses of H_2 and O_2 evolution during photoirradiation from aqueous EtOH solution on (a-i) Rh_2O_3 (0.5 wt %)/$SrTiO_3$:Sc and (a-ii) Ta_2O_5 (5 wt %)/Rh_2O_3 (0.5 wt %)/$SrTiO_3$:Sc. (b-i,ii) Schematic of the reaction mechanism in aqueous EtOH solution. Catalyst, 0.1 g; solution, aq. MeOH (10 vol %, 250 mL); light source, Xe lamp (300 W, full arc). Filled circles, H_2; filled triangles, O_2.

Ta_2O_5 covered almost the whole surface of $SrTiO_3$:Sc particles at this loading amount and mostly prevented the access of EtOH molecules to the $SrTiO_3$:Sc surface. On the other hand, H_2O molecules could reach the $SrTiO_3$:Sc surface by permeation and were oxidized by holes at the interface between the coating layer and $SrTiO_3$:Sc, resulting in O_2 generation via water oxidation, as schematically illustrated in Figure 6b-i,ii. This rules out the possibility that hole migration to the outer surface of the Ta_2O_5 layer by direct excitation of Ta_2O_5 or by hole injection from $SrTiO_3$:Sc may have contributed to photocatalysis. These results strongly support the proposed reaction model.

Thus, the photodeposition process seems not to be necessarily indispensable if a fully covered surface structure is fabricated. On the basis of this idea, various other coating methods were examined (see Supporting Information SI7). Among these methods, the above in situ photodeposition method showed the highest photocatalytic activity.

3.2. Photodeposition above Full Coverage. The above results revealed that the surface of the photocatalyst particles was almost fully covered at 5 wt % of Ta_2O_5 photodeposition. Further Ta_2O_5 photodeposition above full coverage was examined to investigate the behavior of the photodeposition and water splitting reactions. Figure 7 shows the time course of gas evolution during an attempt of larger amounts of Ta_2O_5 (5 + 5 + 5 wt %) deposition and the subsequent water splitting process. Addition of the Ta source was carried out in three steps of 5 wt % each. O_2 evolution occurred as a result of the decomposition of H_2O_2 and Ta peroxide in the initial

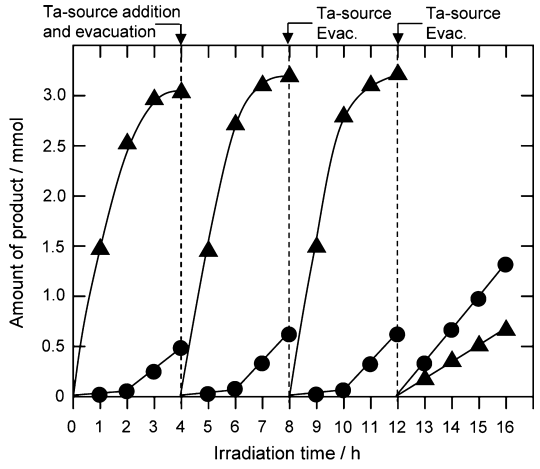

Figure 7. Time courses of gas evolution during photodeposition of Ta_2O_5(5 + 5 + 5 wt %) and subsequent water splitting reactions on Rh_2O_3 (0.5 wt %)/$SrTiO_3$:Sc. Catalyst, 0.1 g; solution, H_2O (250 mL); light source, Xe lamp (300 W, full arc). Filled circles, H_2; filled triangles, O_2.

photodeposition process and continued even after the second photodeposition process.

ICP analysis revealed that the net amounts of deposited Ta_2O_5 were 2.7 and 3.3 wt % for 5 and 15 wt % additions, respectively. This result indicates that the surface of photocatalyst particles reached a full coverage at around 3 wt % deposition, and the successive deposition of Ta_2O_5 was almost prevented. The excessive amount of Ta species remained in the solution likely as a form of oxide cluster. This is in similar phenomenon to the case of Cr_2O_3 photodeposition. According to our previous studies on Cr_2O_3 photodeposition, deposition terminated within a thickness of a few nanometers, even when the amount of Cr source addition was increased, because no electron transport occurred in the Cr_2O_3 layer.[21,22]

The observed O_2 evolution during the whole photodeposition process indicates that H_2O_2 decomposition was not prevented after the full coverage. At present, we interpret this to mean that the H_2O_2 is sorbed into the coating layer and decompose there, rather than that photoexcited carriers react with H_2O_2 on the external surface of the coating layer via charge transport from $SrTiO_3$:Sc to the coating layer. The rationale behind this interpretation is as follows. First, the injection of photocarriers in the Ta_2O_5 layer would be unlikely because the layer's conduction band minimum is more negative than that of $SrTiO_3$:Sc. An electron tunneling model is also improbable because the layer growth was prevented after the full coverage with a few nanometers thickness. Second, given that the coating component Ta_2O_5 could be dissolved in aqueous H_2O_2, the affinity of H_2O_2 for the coating layer must be high, which would allow the sorption into the coating layer.

3.3. Photodeposition Mechanism. During the photodeposition process, the decomposition of metal peroxide complexes likely occurs in competition with H_2O_2 decomposition, which can be monitored only via O_2 evolution. Therefore, the decompositions of the two peroxide species are not distinguishable. For simplicity, the photodecomposition mechanism of the metal peroxide is discussed in connection with the photodecomposition of H_2O_2, assuming that both processes occur by a similar mechanism. As mentioned in the Introduction peroxides are in the O^- valence state, which could easily be reduced to the stable valence state O^{2-}. In this case,

DOI: 10.1021/jacs.5b04107
J. Am. Chem. Soc. 2015, 137, 9627−9634

peroxide functions as an oxidant. On the other hand, especially in a basic aqueous medium, peroxide is known to function as a reductant, where the O^- state is oxidized to the O^0 state, generating O_2. The reaction steps representing these valence changes in the oxygen species in peroxides are given by the following equations, using H_2O_2 as an example.

H_2O_2 as an electron acceptor:

$$H_2O_2 + 2H^+ + 2e^- \rightarrow 2H_2O \quad (5)$$

H_2O_2 as an electron donor:

$$H_2O_2 + 2h^+ \rightarrow O_2 + 2H^+ \quad (6)$$

Overall reaction:

$$2H_2O_2 + 2(e^- + h^+) \rightarrow O_2 + 2H_2O \quad (7)$$

Eqs 5 and 6 represent the cases where H_2O_2 functions as an oxidant and reductant, respectively. The overall reaction, i.e., the sum of eqs 5 and 6, is given by eq 7. The standard electrode potentials for eqs 5 and 6 are 1.77 and 0.68 V (versus NHE, at pH = 0), respectively.[31] Thermodynamically, reduction or oxidation of H_2O_2 should be far easier than H^+ reduction or water oxidation (0, 1.23 eV versus NHE at pH = 0), respectively. Therefore, upon photoirradiation, the decomposition of peroxide species occurs preferentially over water splitting. Assuming that the decompositions of H_2O_2 and metal peroxide complexes occur by a similar mechanism, metal peroxides could also be decomposed reductively on the cocatalyst surface by photoexcited electrons, and oxidatively on the bare surface of the semiconductor photocatalyst by holes. This is likely the reason why the photocatalyst particle surfaces were completely coated with the deposited material to create a core–shell-structured photocatalyst.

The present photodeposition method has a number of advantages over Cr_2O_3 photodeposition, as demonstrated in our recent report.[26] The decomposition of peroxide is a downhill reaction, which can proceed more easily than the uphill reaction of Cr_2O_3 photodeposition from CrO_4^{2-}. Therefore, the photodeposition from the peroxide complex could be performed even on a narrower-gap photocatalyst with weaker reduction and oxidation forces, which is one conceivable advantage of this method. In fact, it was demonstrated that the present photodeposition effected overall water splitting on a narrow-gap (2.08 eV) photocatalyst, $LaMg_{1/3}Ta_{2/3}O_2N$, while Cr_2O_3 photodeposition did not. Another advantage of the present surface modification was that covering the water oxidation sites on the oxynitride photocatalyst with a coating stabilized the photocatalyst surface against photo-oxidative degradation. Thus, the present surface modification method is expected to pave the way to the development of various new visible-light-driven photocatalysts for overall water splitting.

3.4. Water Splitting Mechanism. With respect to the function of the coating layer, it can be concluded that the coating layers functioned neither as a photosensitizer nor as a photocatalyst nor as an electron/hole-transport layer, but rather as a molecular sieve to control the surface redox reactions. The deposited Ta_2O_5 is amorphous and likely hydrated in water, and thus the reactant H^+ ions and H_2O molecules can be supplied to the reaction site.

In the present reaction model, O_2 molecules, generated at the interface between the $SrTiO_3$:Sc particles and Ta_2O_5 layer by a reaction with hydrated water and holes, need to be released from the coating layer. The O_2 molecules generated are temporarily confined to an extremely narrow space, in which the partial pressure of O_2 presumably becomes very high, leading to the release of O_2 from the coating layer by penetration. Since the coating layer is amorphous and a low-density material, it does not hinder the release of the evolved O_2, because of the lattice flexibility of the amorphous layer. On the other hand, O_2 permeation in the opposite direction is unlikely to occur because the partial pressure of O_2 in the outer phase is lower than that in the coating layer. Thus, only one-way permeation of O_2 is possible. This selective permeability of the coating layer prevented the reverse reaction without suppressing the forward reaction, enabling overall water splitting.

This function, derived from the core–shell-structured photocatalyst, is effective for overall water splitting, and could be a model structure for performing photocatalytic overall water splitting. The permeation behavior of the coating layer for various reactant and product molecules is illustrated in Figure 8, along with the mechanism for overall water splitting.

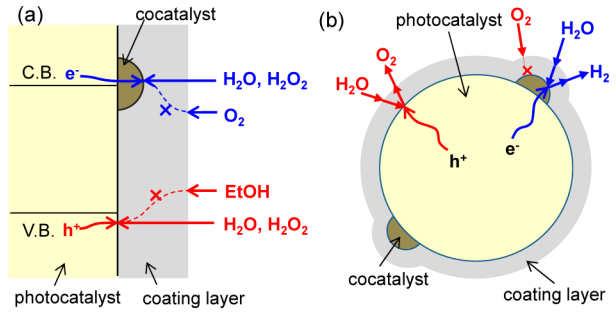

Figure 8. Schematics of (a) permeation behavior, and (b) reaction mechanism for overall water splitting on core–shell-structured photocatalyst.

H_2O and H_2O_2 can likely be incorporated into the coating layer, while O_2 and EtOH cannot permeate the layer from the outside. The observed selective permeability indicates a molecular sieving function of the coating layer. Generally, molecular sieving functions arise from a regulated pore size and/or polarity.[32,33] It is not an easy task to determine the detailed structure of the coating layer because it is very thin and amorphous. Nevertheless, it is certain that the coating layer has no regulated porous structure like zeolites. Although the molecular size of H_2O_2 is larger than that of O_2, H_2O_2, but not O_2, can be incorporated into the coating layer. This result rules out the possibility of a pore-size-induced selective permeability. The results that O_2 and EtOH, which are less polar and hydrophilic, cannot permeate inside indicate a polarity-induced molecular sieving function. Thus, the observed selective permeability is most likely the result of the hydrophilicity of the coating layer.

SUMMARY

An effective novel method for surface modification of photocatalysts for water splitting was devised. Photodeposition of metal (Ti, Nb, Ta) oxyhydroxides from the corresponding metal peroxides enabled the formation of core–shell-structured photocatalysts, in which the whole surface of each photocatalyst particle was coated with the deposited material. The homogeneous coating likely resulted from the facile reductive and oxidative decompositions of peroxides on the photocatalyst

DOI: 10.1021/jacs.5b04107
J. Am. Chem. Soc. 2015, 137, 9627–9634

surface. This unique structure was demonstrated to be effective for overall water splitting even though the reaction sites were covered by the coating, because of the coating's selective permeation behavior: H_2O was allowed to permeate in, while the produced gases were allowed to permeate out. This molecular sieving function enabled the control of concurrent multiple reaction steps, namely, the prevention of the reverse reaction without suppressing the forward reaction, leading to successful overall water splitting. Although the concept of kinetic control by a molecular sieve itself is not new in the field of catalysis, its effective application to photocatalytic water splitting is unprecedented and promises to have a strong impact. Since water splitting is thermodynamically far more unfavorable than water formation, kinetic control is the most logical means to overcome the thermodynamic constraint. It is expected that the findings of the present study can be extended to other photocatalytic materials and pave the way to new material designs, in our own future research as well as that of others.

■ ASSOCIATED CONTENT

Supporting Information

Additional experimental data and discussion pertaining to $SrTiO_3$:Sc; additional experimental data for long-term photoirradiation runs; additional experimental data and discussion pertaining to Rh cocatalyst core; additional experimental data and discussion pertaining to another photodeposition method; additional experimental data and discussion pertaining to various surface coating methods; additional experimental data for XPS and XRD analysis. The Supporting Information is available free of charge on the ACS Publications website at DOI: 10.1021/jacs.5b04107.

■ AUTHOR INFORMATION

Corresponding Authors

*takata.tsuyoshi@nims.go.jp
*domen@chemsys.t.u-tokyo.ac.jp

Notes

The authors declare no competing financial interest.

■ ACKNOWLEDGMENTS

This work was supported in part by the Development of Environmental Technology using Nanotechnology from the Ministry of Education, Culture, Sports, Science and Technology (MEXT), Grants-in-Aid for Scientific Research (C) (No. 24560953) and for Specially Promoted Research (No. 23000009), the Artificial Photosynthesis Project of the Ministry of Economy, Trade and Industry (METI) and "Nanotechnology Platform" (project No.12024046) from MEXT of Japan. Advice and comments by Prof. Yuichi Ikuhara have been a great help in the structural characterization. We are also grateful to Mr. Yoshihide Yoshida at KRATOS XPS Section, Analytical & Measuring Instruments Division, Shimadzu Corp. for performing XPS analysis, and Material Analysis Station at NIMS for performing the ICP analysis.

■ REFERENCES

(1) Maeda, K.; Domen, K. *J. Phys. Chem. C* **2007**, *111*, 7851−7861.
(2) Kudo, A.; Miseki, Y. *Chem. Soc. Rev.* **2009**, *38*, 253−278.
(3) Osterloh, F. E. *Chem. Mater.* **2008**, *20*, 35−54.
(4) Zong, X.; Yan, H.; Wu, G.; Ma, G.; Wen, F.; Wang, L.; Li, C. *J. Am. Chem. Soc.* **2008**, *130*, 7176−7177.
(5) Lukowski, M. A.; Daniel, A. S.; English, C. R.; Meng, F.; Foricux, A.; Hamers, R.; Jim, S. *Energy Environ. Sci.* **2014**, *7*, 2608−2613.
(6) Faber, M. S.; Lukowski, M. A.; Ding, Q.; Kaiser, N. S.; Jin, S. *J. Phys. Chem. C* **2014**, *118*, 21347−21356.
(7) Ma, W. R.; Wang, C.; Liang, J.; Liu, X.; Zhou, K.; Sasaki, T. *ACS Nano* **2015**, *9*, 1977−1984.
(8) Liu, X.; Zheng, H.; Sun, Z.; Han, A.; Du, P. *ACS Catal.* **2015**, *5*, 1530−1538.
(9) Zaharieva, I.; Chernev, P.; Risch, M.; Klingan, K.; Kohlhoff, M.; Fischer, A.; Dau, H. *Energy Environ. Sci.* **2012**, *5*, 7081−7089.
(10) Kanan, M. W.; Nocera, D. G. *Science* **2008**, *321*, 1072−1075.
(11) Dinica, M.; Surendranath, Y.; Nocera, D. G. *Proc. Natl. Acad. Sci. U. S. A.* **2010**, *107*, 10337−10341.
(12) Sato, S.; White, J. M. *Chem. Phys. Lett.* **1980**, *72*, 83−86.
(13) Domen, K.; Naito, S.; Soma, M.; Ohnishi, T.; Tamaru, K. *J. Chem. Soc., Chem. Commun.* **1980**, 543−544.
(14) Lehn, J.-M.; Sauvage, J.-P.; Ziessel, R.; Hilaire, L. *Isr. J. Chem.* **1982**, *22*, 168−172.
(15) Inoue, Y.; Niiyama, T.; Asai, Y.; Sato, K. *J. Chem. Soc., Chem. Commun.* **1992**, 579−580.
(16) Sayama, K.; Arakawa, H. *J. Chem. Soc., Chem. Commun.* **1992**, 150−152.
(17) Domen, K.; Kudo, A.; Onishi, T. *J. Catal.* **1986**, *102*, 92−98.
(18) Kudo, A.; Sayama, K.; Tanaka, A.; Asakura, K.; Domen, K.; Maruya, K.; Onishi, T. *J. Catal.* **1989**, *120*, 337−352.
(19) Maeda, K.; Teramura, K.; Masuda, H.; Takata, T.; Saito, N.; Inoue, Y.; Domen, K. *J. Phys. Chem. B* **2006**, *110*, 13107−13112.
(20) Maeda, K.; Teramura, K.; Saito, N.; Inoue, Y.; Domen, K. *J. Catal.* **2006**, *243*, 303−308.
(21) Maeda, K.; Teramura, K.; Lu, D.; Saito, N.; Inoue, Y.; Domen, K. *Angew. Chem., Int. Ed.* **2006**, *45*, 7806−7809.
(22) Yoshida, M.; Takanabe, K.; Maeda, K.; Ishikawa, A.; Kubota, J.; Sakata, Y.; Ikezawa, Y.; Domen, K. *J. Phys. Chem. C* **2009**, *113*, 10151−10157.
(23) Lee, Y.; Teramura, K.; Hara, M.; Domen, K. *Chem. Mater.* **2007**, *19*, 2120−2127.
(24) Liu, H.; Yuan, J.; Jiang, Z.; Shangguan, W.; Einaga, H.; Teraoka, Y. *J. Solid State Chem.* **2012**, *186*, 70−75.
(25) Tiwari, D.; Lee, S. M. Ferrate(VI) in the Treatment of Wastewaters: A New Generation Green Chemical. In *Waste Water—Treatment and Reutilization*; García Einschlag, F. S., Ed.; InTech: Rijeka, Croatia, 2011 (DOI: 10.5772/15500).
(26) Pan, C.; Takata, T.; Nakabayashi, M.; Matsumoto, T.; Shibata, N.; Ikuhara, Y.; Domen, K. *Angew. Chem., Int. Ed.* **2015**, *54*, 2955−2959.
(27) Takata, T.; Domen, K. *J. Phys. Chem. C* **2009**, *113*, 19386−19388.
(28) Bayot, D.; Tinant, B.; Devillers, M. *Inorg. Chem.* **2005**, *44*, 1554−1562.
(29) Maeda, K.; Sakamoto, N.; Ikeda, T.; Ohtsuka, T.; Xiong, A.; Lu, D.; Kanehara, M.; Teranishi, T.; Domen, K. *Chem. - Eur. J.* **2010**, *16*, 7750−7759.
(30) Maeda, K.; Teramura, K.; Lu, D.; Takata, T.; Saito, N.; Inoue, Y.; Domen, K. *J. Phys. Chem. B* **2006**, *110*, 13753−13758.
(31) Krishnan, C. V.; Garnett, M.; Chu, B. *Int. J. Electrochem. Sci.* **2008**, *3*, 1348−1363.
(32) Davis, E. M.; Loho, F. R. *Chem. Mater.* **1992**, *4*, 756−768.
(33) Li, B.; Wang, H.; Chen, B. *Chem. - Asian J.* **2014**, *9*, 1474−1498.

DOI: 10.1021/jacs.5b04107
J. Am. Chem. Soc. 2015, 137, 9627−9634